**MATERIALS SCIENCE / МАТЕРИАЛОВЕДЕНИЕ**

**UDC** 669.046:533.9
**DOI** 10.17073/0368-0797-2024-6-702-709



***Original article***
***Оригинальная статья***

# STRUCTURAL-PHASE COMPOSITION AND MECHANICAL PROPERTIES OF STAINLESS STEEL – LOW CARBON STEEL METAL COMPOSITE

**V. I. Danilov[1] ✉, D. V. Orlova[1], G. V. Shlyakhova[1], Yu. P. Mironov[1], E. D. Petrova[2]**

[1] **Institute of Strength Physics and Materials Science, Siberian Branch of the Russian Academy of Sciences** (2/4 Akademicheskii Ave., Tomsk 634055, Russian Federation)
[2] **Saint-Petersburg State Marine Technical University** (3 Lotsmanskaya Str., St. Petersburg 190121, Russian Federation)

✉ dvi@ispms.tsc.ru

***Abstract***. The subject of the study is a metal composite obtained by electric arc surfacing in argon of corrosion–resistant steel on low-carbon steel. Powdered chromium-nickel steel was deposited with an increased content of silicon and molybdenum relative to the traditional composition. In this work, we studied the elemental and structural-phase compositions, as well as the mechanical properties of both components of the material and the composite as a whole in the initial state and after annealing at 680 °C for 3 h. The main part of the corrosion-resistant component is a two-phase austenitic-ferritic mixture with a ratio of 65 % HCC phase and 30 % BCC phase. The material has high microhardness (more than 4000 MPa). The highest microhardness (4550 MPa) is observed in a narrow strip of deposited metal with a width of 25 μm, where the phase composition is represented by martensite (BCC), and austenite is absent. The transition across the boundary into carbon steel is accompanied by a decrease in microhardness to 1225 MPa. Here, a decarbonized zone with a width of 180 μm was formed near the fusion line. The resulting non-equilibrium stress-strain state of the composite led to low strength, low plasticity and brittle fracture of the deposited layer during tensile testing. After annealing, microstructure of the corrosion-resistant component became more uniform in size of both austenitic and ferritic structural elements. As a result of these transformations, internal stresses decreased and microhardness decreased to 3100 MPa. At the same time, the width of the decarbonized zone in the base metal increased. All these changes led to the fact that, although the tensile stress of the annealed material increased by 8 %, and the deformation to rupture – by 27 %, however, nature of the fracture remained brittle and rupture still occurs along the deposited layer. This is determined by the austenitic-ferritic phase composition of the stainless component, which, in turn, is determined by chemical composition of the deposited material.

***Keywords:*** electric arc surfacing, corrosion-resistant steel – carbon steel composite, microstructure, microhardness, phase composition, mechanical properties, annealing

***Acknowledgements:*** The work was performed within the framework of the state assignment of the Institute of Strength Physics and Materials Science SB RAS using the equipment of the Nanotech Center of Collective Use, topic No. FWRW-2021-0011.

***For citation:*** Danilov V.I., Orlova D.V., Shlyakhova G.V., Mironov Yu.P., Petrova E.D. Structural-phase composition and mechanical properties of stainless steel – low carbon steel metal composite. *Izvestiya. Ferrous Metallurgy*. 2024;67(6):702–709.
https://doi.org/10.17073/0368-0797-2024-6-702-709

# Исследование структурно-фазового состава и механических свойств металлокомпозита нержавеющая сталь – низкоуглеродистая сталь

**В. И. Данилов[1], Д. В. Орлова[1], Г. В. Шляхова[1], Ю. П. Миронов[1], Е. Д. Петрова[2]**

[1] **Институт физики прочности и материаловедения Сибирского отделения РАН** (Россия, 634055, Томск, пр. Академический, 2/4)
[2] **Санкт-Петербургский государственный морской технический университет** (Россия, 190121, Санкт-Петербург, ул. Лоцманская, 3)

dvi@ispms.tsc.ru

***Аннотация***. Предмет изучения – металлический композит, полученный электродуговой наплавкой в аргоне коррозионностойкой стали на низкоуглеродистую сталь. Наплавлялась порошковая хромоникелевая сталь с повышенным относительно традиционного состава содержанием кремния и молибдена. В настоящей работе исследованы элементный и структурно-фазовый составы, а также механические свойства обоих компонентов материала и композита в целом в исходном состоянии и после отжига при 680 °С в течение 3 ч. Основная часть коррозионностойкого компонента является двухфазной аустенитно-ферритной смесью с соотношением 65 % ГЦК-фазы и 30 % ОЦК-фазы. Материал обладает высокой микротвердостью (более 4000 МПа). Наибольшая микротвердость (4550 МПа) наблюдается в узком слое наплавленного металла шириной 25 мкм, где фазовый состав представлен мартенситом (ОЦК), а аустенит отсутствует. Переход через границу в углеродистую сталь сопровождается уменьшением микротвердости до 1225 МПа. Здесь вблизи линии сплавления образовалась обезуглероженная зона шириной 180 мкм. Сформировавшееся неравновесное напряженно-деформированное состояние композита привело к низкой прочности, малой пластичности и хрупкому разрушению наплавленного слоя при испытании на растяжение. После отжига микроструктура коррозионностойкого компонента стала более однородной по размерам как аустенитных, так и ферритных структурных элементов. В результате этих преобразований снизились внутренние напряжения и уменьшилась микротвердость до 3100 МПа. В то же время увеличилась ширина обезуглероженной зоны в основном металле. Все эти изменения привели к тому, что, хотя напряжение разрушения при растяжении отожженного материала увеличилось на 8 %, а деформация до разрыва – на 27 %, однако характер разрушения остался хрупким и разрыв по-прежнему происходит по наплавленному слою. Это определяется аустенитно-ферритным фазовым составом нержавеющего компонента, который, в свою очередь, задается химическим составом наплавляемого материала.

***Ключевые слова:*** электродуговая наплавка, композит коррозионностойкая сталь – углеродистая сталь, микроструктура, микротвердость, фазовый состав, механические свойства, отжиг

***Благодарности:*** Работа выполнена в рамках государственного задания Института физики прочности и материаловедения Сибирского отделения РАН с использованием оборудования ЦКП «Нанотех», тема № FWRW-2021-0011.

***Для цитирования:*** Данилов В.И., Орлова Д.В., Шляхова Г.В., Миронов Ю.П., Петрова Е.Д. Исследование структурно-фазового состава и механических свойств металлокомпозита нержавеющая сталь – низкоуглеродистая сталь. *Известия вузов. Черная металлургия*. 2024;67(6):702–709. https://doi.org/10.17073/0368-0797-2024-6-702-709

## Introduction

The strict and often contradictory requirements for materials in specialized mechanical engineering, chemical, nuclear, electrical, and electronics industries frequently make it impossible to rely on existing homogeneous metals and alloys. This challenge has driven the development and widespread adoption of layered metal composites. These composites, widely used in mechanical engineering, are valued for their high structural strength, corrosion resistance, heat resistance, and weldability – all achieved at relatively low cost. In large-scale industrial production, layered metal composites are typically manufactured as sheets, tubes, strips, and rods through casting followed by joint hot rolling of the components [1 – 4]. For applications with limited production volumes, various protective coatings – such as gas-thermal, ion-plasma diffusion, or electroplated coatings – are often more practical [5 – 8].

Among the most commonly used layered metal composites are those featuring a base layer of low-carbon or low-alloy steel, with cladding layers made of corrosion-resistant steel, copper, nickel, titanium, or other metals and alloys. This combination is designed to ensure that the base layer provides the required strength characteristics, while the cladding layer protects against aggressive environmental conditions. A cost-effective and accessible method for producing such composites is electric arc surfacing using a consumable austenitic electrode applied to low-alloy carbon steel [9]. This method makes it possible to create cladding layers with the desired physical and mechanical properties and precise geometric parameters. The use of powdered electrodes has proven particularly effective [10; 11]. Moreover, the process is

compatible with standard welding machines, leveraging well-established operating modes [12].

Despite its advantages, the production of such metal composites is not without challenges. Issues such as residual stresses, anisotropy, and the formation of porosity remain significant concerns. It is well known that during surfacing or welding, the cladding layer can acquire either a cast structure (in single-layer surfacing) or a structure modified by additional thermal treatment in specific zones (in multi-pass surfacing). When corrosion-resistant steel is surfaced onto carbon steel, the fusion zone may form martensitic or austenitic-ferritic structures, depending on the carbon content and diffusion processes [13 – 15]. Insufficient nickel and chromium in the deposited metal can lead to a secondary austenitic-martensitic structure [12]. These structures inevitably contribute to a complex stress state in and around the contact zone. Furthermore, the degree of mixing between the base and deposited metals significantly influences the stress-strain state of the bimetal composite. Ultimately, these factors play a decisive role in determining the overall performance characteristics of the layered metal composite.

This study aimed to assess the structure and stress-strain state of a layered metal composite made from corrosion-resistant steel and low-carbon steel, produced via electric arc surfacing, and to identify optimal thermal treatment parameters to enhance the structural strength of the material.

## Materials and methods

The subject of this study is a metal composite obtained through automatic electric arc surfacing in an argon atmosphere, performed in two passes using a consumable powdered electrode on a plate of standard carbon steel grade 20 (as per GOST 1050–88) [16]. The electrode diameter was 1.5 mm, the plate thickness was 8 mm, the width of the deposited bead was 20 mm, and the average bead height was 10 mm. The chemical composition of the powdered electrode was as follows (wt. %: ≤0.12 C; ~18.0 Cr; ~1.0 Mn; ~5.0 Si; ~9.0 Ni; ~1.0 Mo; ~0.2 Ti; <0.04 S; <0.04 P; with the balance being iron. To prevent cracking during surfacing, the plate was preheated to approximately 300 °C.

For mechanical testing, a series of "*dog bone*" samples were cut from the resulting workpiece along the axis of the bead using the electro-erosion method.

The sample design and the scheme for measuring microhardness and evaluating structural-phase characteristics are shown in Fig. 1. The dimensions of the working section of the sample were 40×6×2 mm. In the working area of the sample, the fractions of the deposited metal and the base metal were approximately equal. Some of the prepared samples were annealed in a vacuum at a temperature of 680 °C for 3 h, followed by furnace

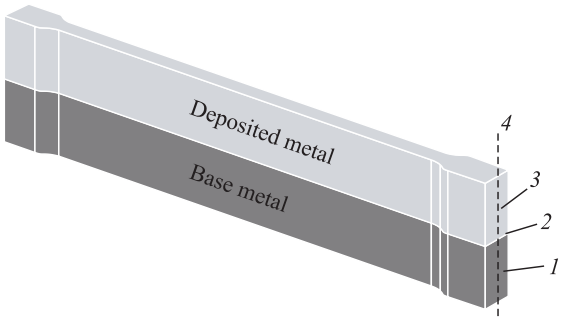


***Fig. 1.*** A sample of metal composite for mechanical testing and determination of structural and phase characteristics: *1* – base metal; *2* – fusion line; *3* – deposited metal; *4* – line for measuring microhardness and certification of structural and phase characteristics

***Рис. 1.*** Образец металлокомпозита для механических испытаний и определения структурно-фазовых характеристик: *1* – основной металл; *2* – линия сплавления; *3* – наплавленный металл; *4* – линия измерения микротвердости и аттестации структурно-фазовых характеристик

cooling (the initial state of the samples without heat treatment is referred to as "State *1*" and the state after annealing is referred to as "State *2*"). For structural analysis, cross-sectional samples were prepared in accordance with RD 24.200.04–90. The analysis of the cross-sections was conducted using a Neophot-21 microscope (Zeiss, Germany). The elemental composition of the deposited and base metals was determined using a LEO EVO 50 scanning electron microscope (Zeiss, Germany). Microhardness was measured with a PMT-3 microhardness tester (1 N load on the indenter), and phase composition was analyzed with a DRON-8 *X*-ray diffractometer (copper radiation).

Uniaxial tensile tests at room temperature were conducted on a Walter + Bai AG, model LFM-125 machine (Switzerland) at a crosshead speed of 0.2 mm/min.

## Results and discussion

Fig. 2, *a* shows the macrostructure of the metal composite sample in State *1*. A strongly etched fusion boundary is distinctly visible. The deposited metal exhibits a layered structure with well-defined boundaries (Fig. 2, *a*). The layers are numbered starting from the fusion boundary, and their dimensions are provided in Table 1.

*Table 1.* **Layers of deposited metal**

*Таблица 1.* **Слои наплавленного металла**

| Sample state | Layer thickness, mm | | | |
|---|---|---|---|---|
| | *I* | *II* | *III* | *IV* |
| Initial (*1*) | 0.025 | 1.50 | 1.35 | 1.25 |
| After annealing (*2*) | 0.050 | 1.10 | 1.90 | 1.30 |

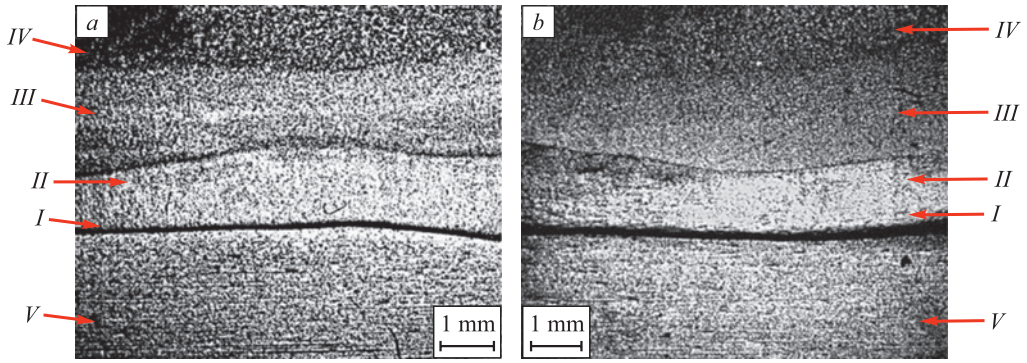


***Fig. 2.*** Macrostructural image of the metal composite:
*a* – initial state; *b* – state after annealing; *I – IV* – layer of deposited metal; *V* – base metal

***Рис. 2.*** Макроструктурное изображение металлокомпозита:
*a* – исходное состояние; *b* – состояние после отжига; *I – IV* – слои наплавленного металла; *V* – основной металл

Layer *I* is located immediately adjacent to the fusion line, where the deposited metal underwent the most significant structural and phase transformations. The material in this layer etches poorly, giving it an unstructured appearance. The formation of such "white zones" is typical for welded joints between high-alloy corrosion-resistant steels and carbon steels. According to previous studies [17 – 19], these zones exhibit a martensitic structure. In the macroscopic image (Fig. 2, *a*), layers *II* and *III* appear visually similar but are separated by a clearly distinguishable boundary.

Microstructural analysis revealed that in State *1*, the deposited metal has a cast structure, with the size and morphology of structural elements differing across layers *II – IV* (Fig. 3, *a*). In layers *II* and *III*, the deposited metal displays a dendritic structure with dark inter-dendritic regions. Near the boundary between layers *I* and *II*, the dendrites transition into polyhedral grains, while the inter-dendritic regions transform into inter-granular boundaries. The boundary of layer *I* is marked with a red dashed line in Fig. 3. As the boundary of layer *III* is approached, the thickness of the inter-dendritic regions increases, the transverse size of the dendrites decreases, and dark particles begin to form within them. Overall, in layer *III*, the dendritic structure is most pronounced and relatively uniform. The structure of layer *IV* is heterogeneous. The transverse sizes of the dendrites can vary significantly, differing by several times. The dark regions between the dendrites are spatially oriented and appear to have a phase composition distinct from that of the dendrites themselves.

Figs. 2, *a* and 3, *a* show that the macro- and microstructure of the base metal (layer *V*) is generally typical. The microstructure corresponds to that of high-quality carbon steel grade 20, consisting of polyhedral ferrite grains with a small amount of pearlite (Fig. 3, *a*). In State *1*, the average grain size was 21 ± 5 μm, corresponding to a grain size number of 8 ÷ 9. Notable struc-

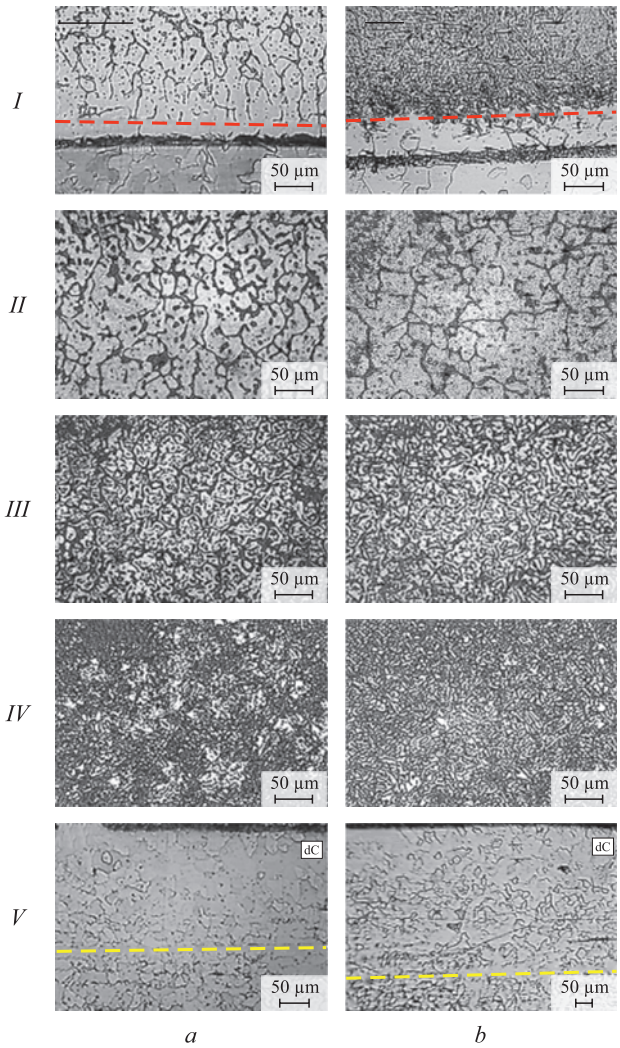


***Fig. 3.*** Microstructure in layers *I – IV* of the deposited metal and base metal *V*:
*a* – initial state *1*; *b* – state after annealing *2*;
*dC* – decarburized zone of the base metal

***Рис. 3.*** Микроструктура в слоях *I – IV* наплавленного металла и основного металла *V*:
*a* – исходное состояние *1*; *b* – состояние после отжига *2*;
dC – обезуглероженная зона основного металла

tural changes were observed near the fusion line, where a decarbonized zone (dC) formed, characterized by the absence of pearlite. This zone is 180 μm wide, with its boundary indicated by a yellow dashed line in Fig. 3.

The microhardness of the composite varies according to the structural characteristics of its layers (Fig. 4, curve *1*). The deposited metal exhibits a microhardness more than double that of the base metal, approximately 4000 MPa compared to 1700 MPa. The highest microhardness, 4550 MPa, is observed in the non-etching layer *I*. Moving toward the middle of layer *II*, the microhardness decreases but begins to rise again, reaching a nominal value of about 4000 MPa in layer *III*. At the fusion boundary, the microhardness measures 2550 MPa, while its lowest value of 1225 MPa corresponds to the decarbonized zone (dC) in the base metal.

The structural characteristics of the deposited metal layers and the microhardness distribution are closely tied to changes in phase composition. Fig. 5 shows the diffraction pattern obtained for the main portion of the deposited metal (curve *1*), indicating the presence of two dominant phases: FCC and BCC. At the farthest distance from the fusion boundary (layer *IV*), the FCC phase (~65 %, austenite) predominates, while the BCC phase (ferrite) makes up no more 30 %, with no signs of tetragonal distortions. In Fig. 3, *a*, the bright structural elements in layer *IV* are identified as austenite, while the darker, oriented features correspond to ferrite. The remaining ~5 % of the volume consists of a mixture of low-symmetry phases, silicides, and carbides. Near the fusion boundary, the phase composition reverses: in layer I, the BCC phase dominates, while austenite accounts for no more than 5 % of the volume and exhibits significant texturing.

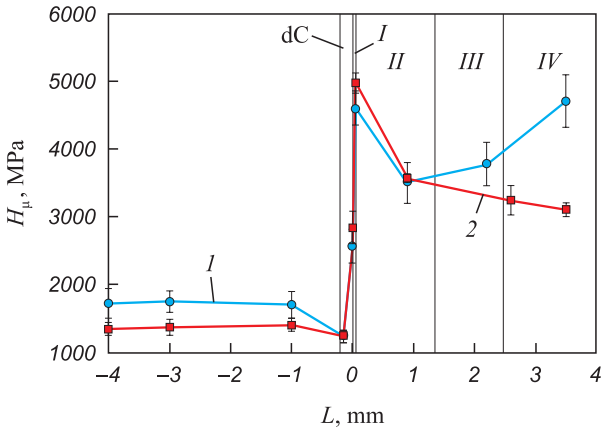


***Fig. 4.*** Microhardness in different layers of the metal composite in initial state (*1*) and after annealing (*2*):
*I – IV* – numbers of layers of deposited metal;
dC – decarburized zone of the base metal

***Рис. 4.*** Микротвердость в разных слоях металлокомпозита в исходном состоянии (*1*) и в состоянии после отжига (*2*):
*I – IV* – слои наплавленного металла;
dC – обезуглероженная зона основного металла

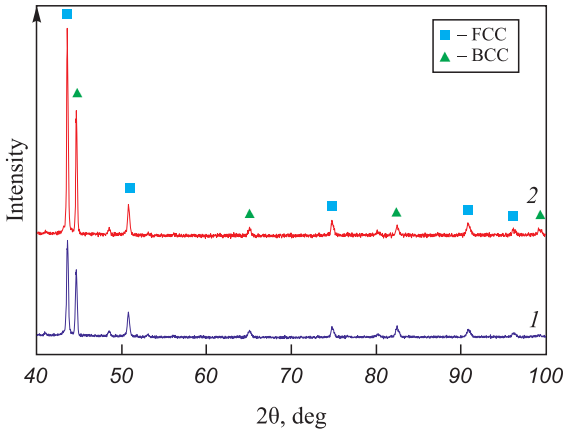


***Fig. 5.*** *X*-ray diffraction patterns of the deposited layer in initial state (*1*) and after annealing (*2*)

***Рис. 5.*** Рентгеновские дифрактограммы наплавленного слоя в исходном состоянии (*1*) и в состоянии после отжига (*2*)

The proportion of low-symmetry phases also decreases to around 2 %. As expected, the base metal consists primarily of the BCC phase. However, near the fusion boundary, the 220 diffraction peaks exhibit significant broadening, likely caused by tetragonal lattice distortions and internal stresses. This observation aligns with previous studies [17; 18] which describe a martensitic structure in the non-etching zone near the fusion boundary.

The observed structural-phase characteristics and microhardness distribution are driven by the diffusion-driven redistribution of carbon and alloying elements near the fusion line (between the base and deposited metals). This is supported by the results of elemental analysis (Table 2).

In layers *III* and *IV* of the deposited metal, the alloying element content closely matches the chemical composition of the powdered electrode. Using the concepts of $Cr_{eq}$ and $Ni_{eq}$ and the A. Schaeffler structural diagram for chromium-nickel stainless steels [20], the two-phase structure of these layers becomes clear. According to this diagram, the FCC phase corresponds to austenite, while the BCC phase corresponds to ferrite. In layer *II*, the nickel content decreases by a factor of three, silicon content by nearly half, and chromium content by half. As a result, the phase composition is a mixture of mar-

*Table 2.* **Chemical composition of the deposited metal**

*Таблица 2.* **Элементный состав наплавленного металла**

| Metal layers | Content of alloying elements, wt. % | | | |
|---|---|---|---|---|
| | Si | Cr | Mn | Ni |
| *III – IV* | 5.4 | 15.3 | 1.3 | 10.3 |
| *II* | 3.3 | 7.6 | 1.6 | 3.6 |
| *I* | 1.8 | 5.2 | 1.5 | 1.8 |

tensite and austenite, consistent with microstructural analysis findings. In layer *I*, the chromium and silicon content drops by a factor of three, and the nickel content decreases by a factor of 5.5, leaving only martensite. This result aligns with both microstructural observations and *X*-ray diffraction analysis.

The analysis of structure, microhardness, *X*-ray diffraction, and elemental composition in the initial State *1* reveals a significant heterogeneity in the material's stress-strain state, which adversely affects the composite's structural strength. The stress-strain curve from uniaxial tensile testing is shown in Fig. 6 (curve *1*). The material displays low plasticity, which is unusual for both carbon and stainless steels. At a strain of ε = 3.6 %, the deposited layer fails, forming a crack that extends through the entire layer. The crack opening reaches up to 1 mm. The diagram shows that the stress calculated for the full cross-section of the composite drops from 554.2 to 219.5 MPa. The base metal layer remains intact and continues to deform plastically. The remaining undamaged cross-sectional area of the sample is 6.33 mm$^2$, meaning that the stress acting in this area equals the stress in the entire sample at the moment the crack forms. This indicates that the failure of the deposited layer is brittle. The low fracture toughness of the deposited layer is likely due to high internal stresses. This issue can be addressed by annealing, which, as described earlier, was performed for 3 h at 680 °C.

The macroscopic image of the annealed material (Fig. 2, *b*) shows that the layered structure of the deposited metal is largely preserved, although the boundary between layers *III* and *IV* is noticeably blurred. The width of layer *I* has increased to 50 μm (Table 1). Layer *I* remains non-etching (Fig. 3, *b*). The adjacent layer *II*, as in State *1*, exhibits a grain structure that gradually transitions into a dendritic structure. The evolution of the microstructure from layer *II* to layer *III* after annealing follows the same pattern observed in the initial state. The dendritic structure of layer *III* remains unchanged between the initial and annealed states. However, significant changes occur in the microstructure of layer *IV* (Figs. 3, *a* and 3, *b*). The microstructure becomes more uniform, with the bright austenitic structural elements becoming more consistent in size, while the dark ferritic elements thicken and lose their preferred orientation.

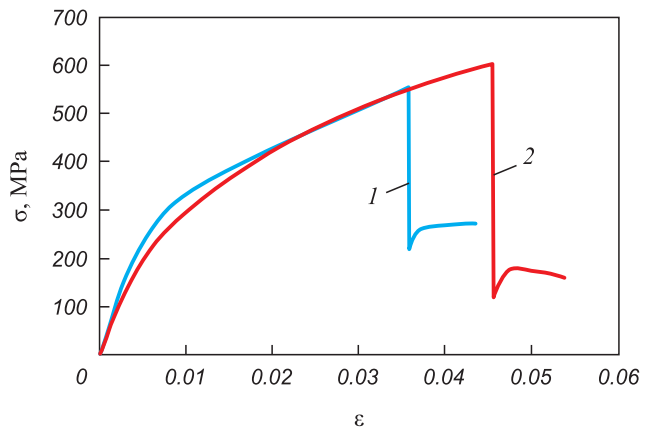


***Fig. 6.*** Loading curves for the composite in initial state (*1*) and after annealing (*2*)

***Рис. 6.*** Диаграммы нагружения композита в исходном состоянии (*1*) и в отожженном состоянии (*2*)

The microhardness distribution of the composite after annealing (State *2*) is shown in Fig. 4, curve *2*. The most notable changes are observed in layer *IV*, where the microhardness decreases from 4700 to 3100 MPa. Conversely, the microhardness of layer *I* increases by 400 MPa compared to the initial state, while the microhardness of the base metal shows a slight decrease. It is also noteworthy that, while the microhardness of the decarbonized zone remains unchanged after annealing, the width of this zone expands to approximately 500 μm.

The phase composition in layers *III* and *IV* remains unchanged after annealing (Fig. 5, *b*), consisting of austenite, ferrite, and less than 5 % of low-symmetry phases. The half-width of the main peaks for the BCC and FCC phases decreases compared to the initial state, indicating a reduction in second-order internal stresses. Furthermore, in layer *I*, the content of the FCC phase decreases significantly (to about 2 %), and the proportion of low-symmetry phases drops to less than 2 %. After annealing, the base metal consists of a more refined BCC phase, reflecting the absence of elastic distortions.

Overall, the deposited metal, fusion boundary, and the composite as a whole transition to a more equilibrated stress-strain state, which has a positive effect on the material's structural strength. As shown by curve *2* in Fig. 6, while the deposited metal still fractures in a brittle manner, the tensile stress at failure increases to 603 MPa, and the relative elongation improves to 4.56 %.

## Conclusions

Studies of the composite produced by electric arc surfacing in an argon atmosphere, combining stainless steel and low-carbon structural steel, showed that the corrosion-resistant component has a two-phase austenitic-ferritic structure. The component features a dendritic structure, with an elemental composition matching that of the electrode wire. The ferritic phase is concentrated in the inter-dendritic regions. Closer to the fusion boundary, the dendritic structure transitions into a grain structure, and the FCC phase content decreases to zero. At the same time, the concentration of alloying elements drops by a factor of 3 to 5, resulting in the formation of a martensitic structure within a few micrometers of the fusion boundary. Overall, the deposited layer exhibits high hardness and brittleness due to significant internal stresses.

Annealing at 680 °C for 3 h improves the microstructure of the deposited layer, reduces hardness, and increases relative elongation at failure. However, the composite remains brittle.

During electric arc surfacing of the corrosion-resistant layer onto low-carbon steel grade 20, a porosity-free layer is formed that is strongly bonded to the base metal. This layer exhibits an austenitic-ferritic phase composition with substantial internal stresses, leading to brittle fracture under load. This brittleness is attributed to the elevated silicon and molybdenum content in the powdered electrode wire compared to traditional compositions for chromium-nickel stainless steels. Although annealing relieves internal stresses in the deposited layer, it does not fully eliminate the composite's brittleness.

## References / Список литературы


1. Golovanenko S.A., Meandrov L.V. Bimetal Production. Moscow: Metallurgiya; 1966:297. (In Russ.).

   Голованенко С.А., Меандров Л.В. Производство биметаллов. Москва: Металлургия; 1966:297.
2. Dhib Z., Guermazi N., Gaspérini M., Haddar N. Cladding of low-carbon steel to austenitic stainless steel by hot-roll bonding: Microstructure and mechanical properties before and after welding. *Materials Science and Engineering: A*. 2016;656:130–141. http://doi.org/10.1016/j.msea.2015.12.088
3. Hu K., Xia Y., Zhu F., Noda N.A. Evaluation of thermal breakage in bimetallic work roll considering heat treated residual stress combined with thermal stress during hot rolling. *Steel Research International*. 2017;89(4):1700368. http://doi.org/10.1002/srin.201700368
4. Mittler T., Greb T., Feistle M., Krinninger M., Hofmann U., Riedle J., Golle R., Volk W. Fabrication and processing of metallurgically bonded copper bimetal sheets. *Journal of Materials Processing Technology*. 2019;263:33–41. https://doi.org/10.1016/j.jmatprotec.2018.08.008
5. Hocking M.G., Vasantasree V., Sidky P.S. Metallic and Ceramic Coatings. NY: Longman Scientific & Technical Publisher; 1989:670.

   Хокинг М., Васантасри В., Сидки П. Металлические и керамические покрытия: Получение, свойства и применение / Под ред. Р.А. Андриевского. Москва: Мир; 2000:518.
6. Khmelevskaya V.B., Moseiko E.S., Ol'khovik E.O. Study of strengthening of ship propeller parts by plasma spray coating with ultrasonic treatment. *Vestnik gosudarstvennogo universiteta morskogo i rechnogo flota im. admirala S.O. Makarova*. 2013;(3):81–87. (In Russ.).

   Хмелевская В.Б., Мосейко Е.С., Ольховик Е.О. Исследование упрочнения деталей судового валопровода методом покрытия плазменным напылением с ультразвуковой обработкой. *Вестник государственного университета морского и речного флота им. адмирала С.О. Макарова*. 2013;(3):81–87.
7. Monceau D., Oquab D., Estournes C., Boidot M., Selezneff S., Ratel-Ramond N. Thermal barrier systems and multi-layered coatings fabricated by spark plasma sintering for the protection of Ni-base superalloys. *Materials Science Forum*. 2010;654–656:1826–1831. https://doi.org/10.4028/www.scientific.net/MSF.654-656.1826
8. Gotz W., Heinisch T. Leyendecker: Steckverbinder – Hohe Zuverlässigkeit bei reduziertem Edelmetalleinsatz. *Galvanotechnik*. 2003;4(9):2139–2140. (In Germ.).
9. Bandyopadhyay A., Heer B. Additive manufacturing of multi-material structures. *Materials Science and Engineering: R: Reports*. 2018;129:1–16. https://doi.org/10.1016/j.mser.2018.04.001
10. Kozyrev N.A., Kibko N.V., Umanskii A.A., Titov D.A. Improving the quality of deposited layer of rolling rolls by optimizing the composition of flux-cored wires. *Svarochnoe proizvodstvo*. 2017;7:29–34. (In Russ.).

    Козырев Н.А., Кибко Н.В., Уманский А.А., Титов Д.А. Повышение качества наплавленного слоя прокатных валков за счет оптимизации состава порошковых проволок. *Сварочное производство*. 2017;(7):29–34.
11. Usol'tsev A.A., Kozyrev N.A., Bashchenko L.P., Kryukov R.E., Zhukov A.V. Development of flux-cored wire of Fe–C–Si–Mn–Cr–W–V system with additives of carbon-fluorine-containing material and titanium. *Izvestiya. Ferrous Metallurgy*. 2023;66(4):403–409. https://doi.org/10.17073/0368-0797-2023-4-403-409

    Усольцев А.А., Козырев Н.А., Бащенко Л.П., Крюков Р.Е., Жуков А.В. Разработка порошковой проволоки системы Fe–C–Si–Mn–Cr–W–V с присадками углеродфторсодержащего материала и титана. *Известия вузов. Черная металлургия*. 2023;66(4):403–409. https://doi.org/10.17073/0368-0797-2023-4-403-409
12. Sidorov V.P., Mel'zitdinova A.V. Methodology for determining the requirements for welding parameters accuracy. *Svarka i diagnostika*. 2014;(3):10–13. (In Russ.).

    Сидоров В.П., Мельзитдинова А.В. Методика определения требований к точности параметров сварки. *Сварка и диагностика*. 2014;(3):10–13.
13. Boronenkov V.N., Korobov Yu.S. Basics of Arc Metallization. Physico-Chemical Patterns. Ekaterinburg: Izd. Ural. un-ta; 2012:268. (In Russ.).

    Бороненков В.Н., Коробов Ю.С. Основы дуговой металлизации. Физико-химические закономерности. Екатеринбург: Изд. Урал. ун-та; 2012:268.
14. Zernin E.A., Petrova E.D., Danilov V.I., Shlyakhova G.V. Structure and properties of a metal deposited by a powder wire in a plasma stream. *Svarka i diagnostika*. 2024;(2):28–33. (In Russ.). https://doi.org/10.52177/2071-5234_2024_02_28

    Зернин Е.А., Петрова Е.Д., Данилов В.И., Шляхова Г.В. Структура и свойства металла, наплавленного порошковой проволокой в потоке плазмы. *Сварка и диагностика*. 2024;(2):28–33. https://doi.org/10.52177/2071-5234_2024_02_28
15. Wielage B., Pokhmurska H., Student M., Gvozdeckii V., Stupnyckyj T., Pokhmurskii V. Iron-based coatings arc-sprayed with cored wires for applications at elevated temperatures. *Surface & Coatings Technology*. 2013; 220:27–35. https://doi.org/10.1016/j.surfcoat.2012.12.013
16. Sorokin V.G., etc. Steels and Alloys. Grade Guide: Reference Book. Moscow: Intermet Inzhiniring; 2001:608. (In Russ.).

    Стали и сплавы. Марочник: Справ. изд. / В.Г. Сорокин и др. Москва: Интермет Инжиниринг; 2001:608.

**17.** Gel'man A.S., Chudnovskii A.D., Tsemakhovich B.D., Kharin I.L. Cladding of Steel by Explosion. Moscow: Mashinostroenie; 1978:191. (In Russ.).

Плакирование стали взрывом / Под ред. А.С. Гельмана, А.Д. Чудновского, Б.Д. Цемаховича, И.Л. Харина. Москва: Машиностроение; 1978:191.

**18.** Trudov A.F., Trykov Yu.P., Klochkov S.V., Dontsov D.Yu., Voinov M.O. The effect of heat treatment on the structural and mechanical heterogeneity of explosion-welded bimetal St.3+12Kh18N10T. *Deformatsiya i razrushenie materialov*. 2009;12:41–44. (In Russ.).

Трудов А.Ф., Трыков Ю.П., Клочков С.В., Донцов Д.Ю., Войнов М.О. Влияние термообработки на структурно-механическую неоднородность сваренного взрывом биметалла Ст.3+12Х18Н10Т. *Деформация и разрушение материалов*. 2009;(12):41–44.

**19.** Shlyakhova G.V., Barannikova S.A., Bochkareva A.V., Li Yu.V., Zuev L.B. Study of the structure of bimetal construction carbon steel – stainless steel. *Izvestiya. Ferrous Metallurgy*. 2018;61(4):219–223. (In Russ.). https://doi.org/10.17073/0368-0797-2018-4-300-305

Шляхова Г.В., Баранникова С.А., Бочкарёва А.В., Ли Ю.В., Зуев Л.Б. Исследование структуры биметалла конструкционная углеродистая сталь – нержавеющая сталь. *Известия вузов. Черная металлургия*. 2018;61(4):300–305. https://doi.org/10.17073/0368-0797-2018-4-300-305

**20.** Schaeffler M. Constitution diagram for stainless steel weld metal. *Metal Progress*. 1949:56:680–681.

## Information about the Authors / Сведения об авторах

***Vladimir I. Danilov,*** *Dr. Sci. (Phys.-Math.), Prof., Chief Researcher of the Laboratory of Strength Physics*, Institute of Strength Physics and Materials Science, Siberian Branch of the Russian Academy of Sciences
***ORCID:*** 0000-0002-5741-7574
***E-mail:*** dvi@ispms.ru

***Dina V. Orlova,*** *Cand. Sci. (Phys.-Math.), Research Associate of the Laboratory of Strength Physics*, Institute of Strength Physics and Materials Science, Siberian Branch of the Russian Academy of Sciences
***ORCID:*** 0000-0003-0068-2542
***E-mail:*** dvo@ispms.ru

***Galina V. Shlyakhova,*** *Cand. Sci. (Eng.), Research Associate of the Laboratory of Strength Physics*, Institute of Strength Physics and Materials Science SB RAS
***ORCID:*** 0000-0001-9578-2989
***E-mail:*** shgv@ispms.ru

***Yurii P. Mironov,*** *Cand. Sci. (Phys.-Math.), Research Associate of the Laboratory of Materials Science of Shape Memory Alloys*, Institute of Strength Physics and Materials Science SB RAS
***ORCID:*** 0000-0002-2351-3592
***E-mail:*** myp@ispms.ru

***Ekaterina D. Petrova,*** *Assistant of the Chair of Welding of Ship Structures*, Saint-Petersburg State Marine Technical University
***ORCID:*** 0009-0002-2302-8359
***E-mail:*** petrowa.ket@yandex.ru

***Владимир Иванович Данилов,*** *д.ф.-м.н., профессор, главный научный сотрудник лаборатории физики прочности*, Институт физики прочности и материаловедения Сибирского отделения РАН
***ORCID:*** 0000-0002-5741-7574
***E-mail:*** dvi@ispms.ru

***Дина Владимировна Орлова,*** *к.ф.-м.н., научный сотрудник лаборатории физики прочности*, Институт физики прочности и материаловедения Сибирского отделения РАН
***ORCID:*** 0000-0003-0068-2542
***E-mail:*** dvo@ispms.ru

***Галина Витальевна Шляхова,*** *к.т.н. научный сотрудник лаборатории физики прочности*, Институт физики прочности и материаловедения Сибирского отделения РАН
***ORCID:*** 0000-0001-9578-2989
***E-mail:*** shgv@ispms.ru

***Юрий Петрович Миронов,*** *к.ф.-м.н., научный сотрудник лаборатории материаловедения сплавов с памятью формы*, Институт физики прочности и материаловедения Сибирского отделения РАН
***ORCID:*** 0000-0002-2351-3592
***E-mail:*** myp@ispms.ru

***Екатерина Дмитриевна Петрова,*** *ассистент кафедры сварки судовых конструкций*, Санкт-Петербургский государственный морской технический университет
***ORCID:*** 0009-0002-2302-8359
***E-mail:*** petrowa.ket@yandex.ru

## Contribution of the Authors / Вклад авторов

***V. I. Danilov*** – formation of the article main concept, scientific guidance, revising and writing the article final version.
***D. V. Orlova*** – analysis and discussion of experimental results, writing the article draft version.
***G. V. Shlyakhova*** – carrying out metallographic studies, describing composite structures.
***Yu. P. Mironov*** – carrying out *X*-ray studies, describing the material phase composition.
***E. K. Petrova*** – performing surfacing in specified modes, obtaining a composite.

***В. И. Данилов*** – идея работы, научное руководство, написание окончательного варианта рукописи.
***Д. В. Орлова*** – анализ и обсуждение экспериментальных результатов, написание первичного варианта рукописи.
***Г. В. Шляхова*** – проведение металлографических исследований, описание структур композита.
***Ю. П. Миронов*** – проведение рентгеновских исследований, описание фазового состава материала.
***Е. К. Петрова*** – выполнение наплавки по заданным режимам, получение композита.

Received 13.08.2024
Revised 05.09.2024
Accepted 20.09.2024

Поступила в редакцию 13.08.2024
После доработки 05.09.2024
Принята к публикации 20.09.2024